

# Chapter 9

## Link Level Measurements

Martin Lerch

Simulators are a powerful tool to evaluate current mobile communications standards and to investigate new transmission and receiver techniques. The next step should then be to perform measurements in a real-world environment. Therefore, a very flexible wireless testbed, the Vienna MIMO Testbed was developed at TU Wien which allows for Long Term Evolution (LTE) measurements including the Vienna LTE-A Link Level Simulators as signal source and receiver. In Sect. 9.2 we provide an overview of the Vienna MIMO Testbed and the methodologies to perform LTE measurements. A measurement campaign that evaluated the impact of the transmit antenna configuration on the performance of the LTE Downlink (DL) is presented in Sect. 9.3. In order to perform reproducible and fully controllable measurements at velocities of up to 400 km/h our testbed was extended by an antenna on a rotary unit. In Sect. 9.4, this unit and the corresponding measurement methodology is described followed by a measurement campaign comparing different channel interpolation techniques for LTE Uplink (UL) transmissions.

### 9.1 Introduction

The decades after Marconi's invention were filled with wireless experiments. Although we understand many physical phenomena of wireless propagations today much better than in the past, our channel models still capture only a part of the complex physical propagation process. Nevertheless, in the last two decades, it has become a common method to entirely skip experimental validation and trust existing channel models when designing mobile communication systems. As the complexity of mobile communication standards also increases, simulation methods appear to be the Holy Grail to address open design questions. While these methods deliver

---

M. Lerch (✉)  
Institute of Telecommunications, TU Wien, Vienna, Austria  
e-mail: mlerch@nt.tuwien.ac.at

quantitative results in acceptable time, many important issues are simplified or not modeled at all, trading off timely results against accuracy. Converting new algorithmic ideas into hardware on the other hand is quite time consuming and often lacks flexibility so that experimental evaluation remains no longer an attractive choice. With our testbed approach [1], we essentially combine the advantages of both worlds: design flexibility and timeliness under true physical conditions.

Although LTE cellular systems are already being rolled out and operated in many countries around the world, there are still unresolved issues in transmission technology. Focusing on point-to-point single-user LTE transmissions, there exist many open questions that can be best tackled by LTE measurements:

- Performance comparison of different kinds of receivers (receiver algorithms),
- Performance of novel and modified transmission schemes following the LTE standard,
- Performance measurements at extreme channels (for example, very high speed) for which channel models are very crude or even nonexistent,
- Comparison of different penetration scenarios or different antenna configurations.

## 9.2 The Vienna MIMO Testbed

Figure 9.1 exhibits the main hardware components of the Vienna MIMO Testbed required to convert a priori generated data into electromagnetic waves, transmit them over the air and finally to capture them before storing them in digital form for further evaluation. The major hardware components are:

- Three rooftop transmitters supporting four antennas each. The digital signal samples are converted with a precision of 16 bits and are transmitted with adjustable power within a continuous range of about  $-35$ – $35$  dBm per antenna.
- One indoor receiver with four channels that converts the received signals with a precision of 16 bits before the raw signal samples are saved to hard disk. The receive

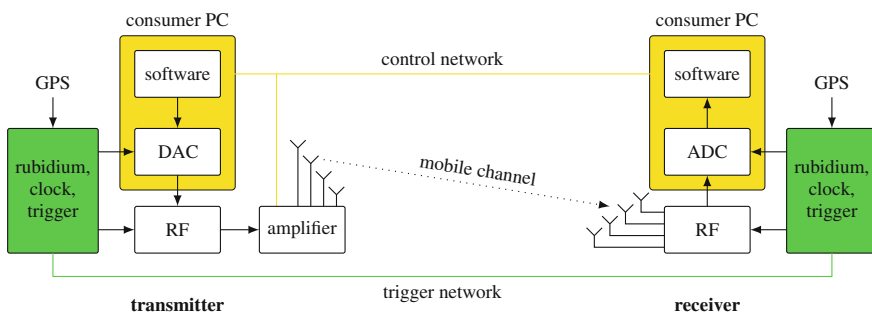


**Fig. 9.1** Major components of the Vienna MIMO testbed

antennas are mounted on a positioning table, which allows for measurements at different positions within an area of about  $1\text{ m} \times 1\text{ m}$ , correspondingly  $8\lambda \times 8\lambda$ .

- The carrier frequency, the sample clock, and the trigger signals are generated separately at each station utilizing Global Positioning System (GPS) synchronized rubidium frequency standards. The synchronization of the triggers is based on exchanging timestamps in the form of User Datagram Protocol (UDP) packets over a trigger network [2]. The precision of this trigger mechanism does not require any further post-synchronization at the receiver. It is sufficient to measure the delay once and time-shift all signals according to the measured delay.
- A dedicated fiber-optic network is utilized to exchange synchronization commands as well as feedback information and general control commands.

The current setup supports a transmission bandwidth of up to 20 MHz at a center frequency of 2.503 GHz.

In typical measurements, the transmission of signals generated according to parameters of interest, is repeated with different values of transmit power in order to obtain results for a certain range of Signal to Noise Ratio (SNR). Furthermore, the transmission of such signals at all values of transmit power is repeated at different receive antenna positions in order to average over small-scale fading scenarios. As a rule of thumb, in a typical scenario approximately 30 measurements of different receive antenna positions are necessary to obtain sound results for an LTE signal with a 10 MHz bandwidth. In order to check whether we have measured sufficient channel realizations, we always include BCa bootstrap confidence intervals in our results [3]. While this process is usually the same for different kinds of measurements, they may differ in the way transmit signals are generated.

As illustrated in Fig. 9.2, we distinguish between two different methodologies as detailed in the following:

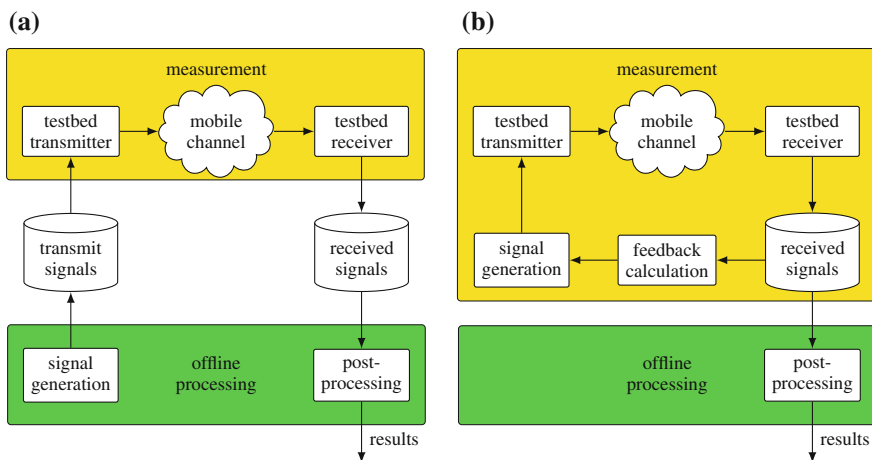


**Fig. 9.2** Methodologies used in LTE measurements: **a** Brute-force approach. **b** Measurements with feedback

- *Brute force measurements*: All signals of interest are pre-generated, transmitted over the physical channel, and saved as raw signal samples to hard disk. The received signals are then evaluated offline. This approach is only feasible as long as the time duration of all the different transmit signals is small compared to the channel variations so that successively transmitted data sets appear to be transmitted over the same channel.
- *Measurements with feedback*: The transmit signals are generated on the fly utilizing channel state information obtained via a preceding transmission of training symbols. While the processing and evaluation of the actual data symbols can be computed offline, the demodulation of the training symbols, evaluation, and decision about the generation of the next transmit signal has to be performed in (quasi-) real time.

While brute force measurements typically take longer than the feedback approach and the number of different signals that need to be evaluated is much higher, results obtained by brute force measurements are typically more detailed and are certainly not contaminated by the quality of the feedback function. If the number of different transmit signals is not too large, a combination of both methodologies is possible. All signals of interest are pre-generated, but only those a feedback function decides for are transmitted. This approach reduces the number of signals that have to be evaluated and signals do not have to be generated during the measurement. Nevertheless, it should be noted that if the number of possible transmit signals is very large (for example, zero-forcing Multi-User MIMO or Interference Alignment (IA) [4]), only a feedback approach is feasible.

### 9.3 Evaluation of LTE MIMO Downlink Transmissions

In different measurement campaigns using Worldwide Inter-Operability for Microwave Access (WiMAX) [5], High-Speed Downlink Packet Access (HSDPA) [6] and LTE [7, 8] the impact of the transmit antenna configuration on the performance of Multiple-Input Multiple-Output (MIMO) transmission modes was investigated. Besides the transmit antenna configuration, the scenario the measurement was performed in has an impact on the performance. Furthermore, the impact of the antenna configuration depends on the receive SNR. In typical field tests, measurements are performed in different scenarios where the SNR is set by the actual scenario. Our approach [9] is different. We fix the scenario and measure over a wide range of transmit power allowing for deeper insights in the impact of the transmit antenna configuration on MIMO transmissions. Thereby, we evaluate the performance of the LTE DL in terms of physical layer throughput on the one hand, and on the other hand, we evaluate the channel capacity as theoretical performance metric.

#### *Measurement Setup*

The measurements were performed in an urban scenario at TU Wien in the city of Vienna, Austria using the MIMO testbed described in Sect. 9.2. The measurement

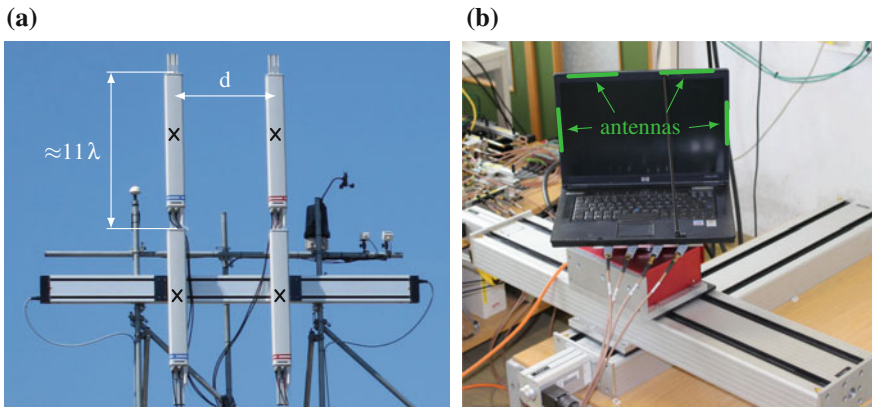


**Fig. 9.3** Measurement setup in downtown Vienna, Austria: **a** Transmitter: Two separately shiftable pairs of vertically stacked antennas allow for measurements at vertical and horizontal transmit antenna configurations. **b** Receiver: A laptop carrying the receive antennas can be moved along the X, Y and  $\Phi$  axis in order to measure different channel realizations

setup is shown in Fig. 9.3 where the transmitter is located outdoors on a rooftop and serves a single user located indoors in the opposite building. In order to implement the desired transmit antenna configurations, we use two pairs of vertically mounted commercial cross polarized antennas that can be moved separately along a linear guide. The four output channels of the transmitter are mapped to four out of the eight antenna elements to transmit with four channels over both, vertically stacked and horizontally spaced antennas. The receive antennas are two horizontally and two vertically polarized custom build patch-antennas mounted around the display of a laptop. This laptop is mounted on a  $XY\Phi$  positioning table and can so be moved within an area of about  $3\lambda \times 3\lambda$  as well as rotated within a range of about  $210^\circ$ .

### *Measurement Methodology*

Measuring at just a single implementation of a transmit antenna configuration neither allows for a fair comparison of different antenna configurations nor does it lead to reproducible results. With our setup, different antenna elements are employed for different antenna configurations. For that reason, we repeat transmissions using all possible implementations of the antenna configurations under investigation. Then, as illustrated in Fig. 9.4, when averaging the results over all possible implementations, the same antenna elements are selected for every antenna configuration. Single antenna results are obtained in a similar way by averaging over the results for all single transmit antenna elements. Furthermore, the transmit antennas are at different positions for different antenna spacings. We, therefore, do not just measure at a single position of the transmit antennas. For every antenna spacing, we repeat the measurement at different random positions along the linear guide and average over the results. At the receiver site, results for different numbers of receive antennas are averaged in a similar way as it is done for the transmit antennas. For  $2 \times 2$

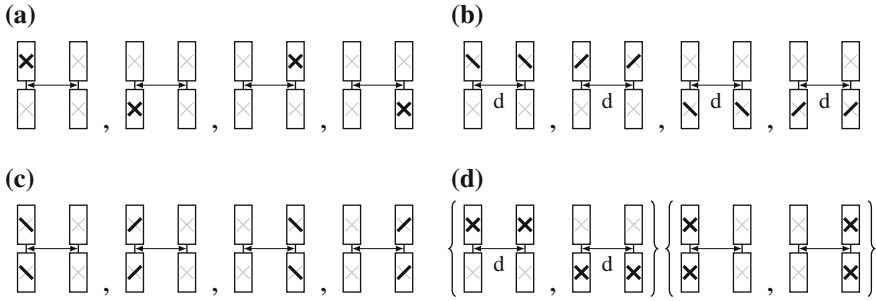


**Fig. 9.4** Averaging over all possible implementations of an antenna configuration allows for a fair comparison with other antenna configurations. Every antenna element is used once for every configuration: **a**  $2 \times 2$  cross polarized, **b**  $2 \times 2$  horizontally spaced, **c**  $2 \times 2$  vertically spaced and **d**  $4 \times 4$  horizontally and vertically spaced

transmissions we average over the results obtained by the first two antennas and the results obtained by the second two antennas. Results for  $1 \times 1$  are averaged over all four available receive antennas. Furthermore, measurements are repeated at different  $XY\Phi$  positions of the receive antennas. Finally, the whole measurement procedure is repeated for different transmit powers. For the generation of the transmit signals and the evaluation after the transmission we modified the Vienna LTE-A Downlink Link Level Simulator [10] to work with the testbed. Thereby, to keep the number of different transmit signals low to use the brute-force approach described in Sect. 9.2, we use the open-loop transmit modes of LTE rather than the closed-loop modes. A summary of all measurement parameters is listed in Table 9.1.

**Table 9.1** Measurement parameters

System bandwidth	10 MHz, scheduled for a single user
Transmission modes	Single antenna, Transmit Diversity (TxD), Open Loop Spatial Multiplexing (OLSM)
Center frequency	2.503 GHz ( $\lambda \approx 12$ cm)
Transmit power	$-13 \dots 35$ dBm
Transmit antennas	$4 \times$ Kathrein 80010541 cross polarized
Transmit antenna spacings	$1.5\lambda, 5.75\lambda, 10\lambda$ (horizontal) $\approx 11\lambda$ (vertical)
Transmit antenna polarizations	$2 \times 2$ : cross polarized (X-pol), equally polarized $4 \times 4$ : double cross polarized

## Evaluation

### 9.3.1 Physical Layer Throughput

By applying the brute-force approach, all possible combinations of Modulation and Coding Schemes (MCSs) and transmission rank  $N_L = \{1, 2, 3, 4\}$  are transmitted and evaluated independently. Thereby, we obtain for every channel realization  $r$ , transmit power  $P_S$  and all combinations of the signal parameters MCSs and  $N_L$  a result in terms of physical layer throughput  $D_r(P_S, \text{MCS}, N_L)$ . The average throughput for a certain antenna configuration is then calculated as the average over all channel realizations  $r$  of the throughput of the respectively best performing combination of MCS and  $N_L$  to

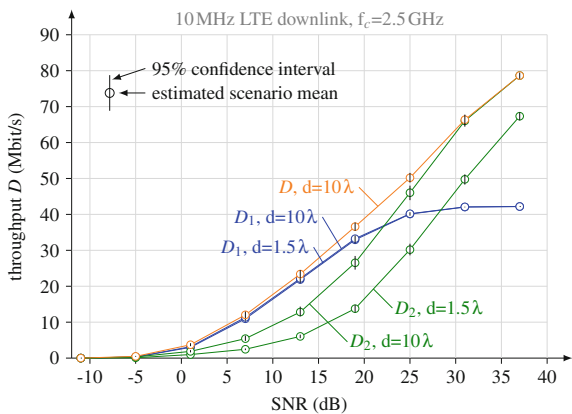
$$D(P_S) = \frac{1}{R} \sum_{r=1}^R \max_{\text{MCS}, N_L} D_r(P_S, \text{MCS}, N_L). \tag{9.1}$$

In order to compare the impact of different antenna configurations in more detail, we furthermore evaluate the throughput for a fixed number of spatial streams  $N_L$ :

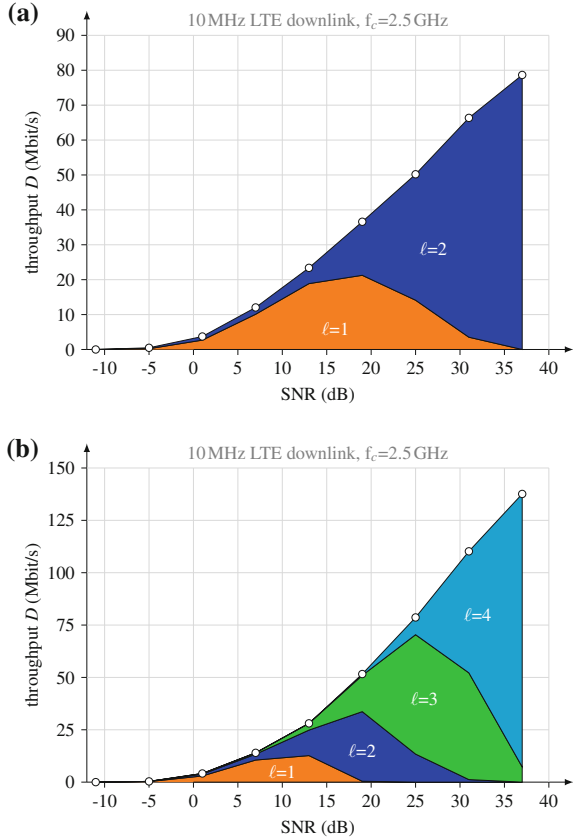
$$D_{N_L}(P_S) = \frac{1}{R} \sum_{r=1}^R \max_{\text{MCS}} D_r(P_S, \text{MCS}, N_L). \tag{9.2}$$

Figure 9.5 shows the measurement results for  $2 \times 2$  transmissions when using equally polarized transmit antennas. If the transmission rank is fixed to  $N_L = 1$ , we do not observe a difference between different antenna spacings. That is different when transmitting two spatial streams ( $N_L = 2$ ). The higher the spacing, the higher the measured throughput  $D_2$ . Furthermore, the average SNR, at which the two-stream transmission outperforms the single-stream transmission is shifted to

**Fig. 9.5** Results for  $2 \times 2$  LTE transmissions: While the performance of single stream transmissions is independent of the antenna spacing, the throughput when transmitting two streams increases with antenna spacing



**Fig. 9.6** Average contribution of rank  $N_L$  transmissions to the average throughput when using rank adaption: **a**  $2 \times 2$  using equally polarized antennas with horizontal spacing of  $d = 10 \lambda$ . **b**  $4 \times 4$  double cross polarized antennas with horizontal spacing of  $d = 10 \lambda$



lower SNRs. The evaluation of  $D$  reflects the technique of rank adaption. In the lower SNR regime, the measured throughput is very close to the throughput for the single-stream transmission. With increasing SNR, the throughput gets close to the throughput of the two-stream transmission. In the region of moderate SNR,  $D$  is higher than the respective throughputs  $D_1$  and  $D_2$ , as we evaluate average throughputs and the break-even point in terms of average SNR differs from channel realization to channel realization. This smooth transition is also shown in Fig. 9.6, where the average contribution of transmissions using  $N_L$  spatial streams to the average total throughput is illustrated. The results for all  $2 \times 2$  antenna configurations when using rank adaption are given by Fig. 9.7. Large differences are only observed at moderate to high SNRs where transmissions with  $N_L = 2$  outperform the single-stream transmissions. Thereby, the throughput increases with antenna spacing  $d$  when using equally polarized transmit antennas. The vertically stacked antennas perform about as good as the horizontally spaced antennas with spacing  $d = 10 \lambda$ . Cross polarized transmit antennas outperform all other antenna configurations. Figure 9.8 shows the results of the  $4 \times 4$  measurements using double cross polarized antennas. As for the



**Fig. 9.7** Results for  $2 \times 2$  LTE transmissions: The best performance for two antenna transmissions is observed when cross polarized antennas are employed

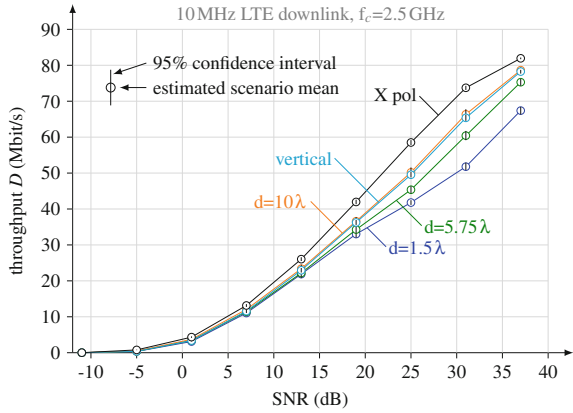
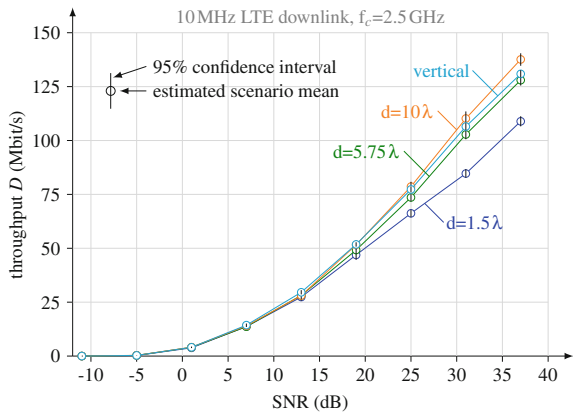


**Fig. 9.8** Results for  $4 \times 4$  LTE transmissions: The performance increases with antenna spacing



$2 \times 2$  case, the performance increases with antenna spacing. The throughput with vertically stacked antennas is close to the throughput for horizontally spaced antennas with  $d = 10\lambda$ .

### 9.3.2 Channel Capacity

Besides results in terms of throughput, the receiver of the LTE simulator provides channel estimates for every subframe transmitted. We evaluate the channel capacity [11] as an upper bound for the data rate by these channel estimates  $\mathbf{H}_k$  measured at the highest transmit power. For an Orthogonal Frequency Division Multiplexing (OFDM) transmission with  $N_c$  subcarriers, a total channel bandwidth  $B$  and  $N_T$  transmit antennas, the channel capacity  $C(P_S)$  as a function of the measured channels  $\mathbf{H}_k$ , the measured noise power  $P_V$  and the transmit power  $P_S$  is given by

$$C(P_S) = \frac{B}{N_c} \sum_{k=1}^{N_c} \log_2 \det \left( \mathbf{I} + \frac{1}{N_T} \frac{P_S}{P_V} \mathbf{H}_k \mathbf{F}_k \mathbf{F}_k^H \mathbf{H}_k^H \right). \quad (9.3)$$

Due to the guard band of 1 MHz specified in the 10 MHz LTE DL,  $\mathbf{H}_k$  is estimated over a bandwidth of 9 MHz only. Therefore, we extrapolate the results to the full bandwidth of  $B = 10$  MHz. Thereby, we assume full Channel State Information (CSI) at the transmitter and use the waterfilling algorithm to calculate the optimal precoder  $\mathbf{F}_k$  for every channel realization. The waterfilling algorithm distributes a fixed value of total transmit power to the available layers according to the eigenvalues  $\lambda_l$  of  $\mathbf{H}_k \mathbf{H}_k^H$ . At low SNRs the maximum is achieved by assigning all power to the strongest eigenvalue. With increasing SNR the number of eigenvalues increases before the available transmit power is assigned equally to all eigenvalues. The eigenvalues obtained by the measurement are listed in Table 9.2 for  $2 \times 2$  and in Table 9.3 for the  $4 \times 4$  channels. A comparison of channel capacity and LTE physical layer throughput for three different transmit antenna configurations for  $2 \times 2$  transmissions is depicted in Fig. 9.9. At low SNRs, both, the capacity and the LTE throughput is independent of the antenna configuration. With increasing SNR, the differences observed for the LTE throughput become visible for the channel capacity in a similar way. The same effects are observed when evaluating the eigenvalues in Table 9.2 where the measured eigenvalues are normalized to the strongest eigenvalue at  $d = 1.5 \lambda$ . Thereby, the strongest eigenvalue  $\lambda_1$  is independent of the transmit antenna configuration while the second eigenvalue  $\lambda_2$  depends on the antenna configuration. The measured eigenvalues for  $4 \times 4$  are listed in Table 9.3 where the two strongest eigenvalues are quite independent of the antenna configuration. The impact of the antenna configuration is visible for the two weakest eigenvalues only.

Finally, we were interested in how much of the channel capacity the LTE physical layer throughput could reach in our measurement. Therefore, we define the

**Table 9.2** Normalized eigenvalues of measured  $2 \times 2$  channels

	$d=1.5 \lambda$ (dB)	$d=5.75 \lambda$ (dB)	$d=10 \lambda$ (dB)	Vertical (dB)	X polarized (dB)
$\lambda_1$	0.0	0.1	0.0	0.0	-0.27
$\lambda_2$	-20.2	-16.5	-14.4	-14.7	-10.9

**Table 9.3** Normalized eigenvalues of measured  $4 \times 4$  channels

	$d=1.5 \lambda$ (dB)	$d=5.75 \lambda$ (dB)	$d=10 \lambda$ (dB)	Vertical (dB)
$\lambda_1$	0.0	0.2	0.1	-0.1
$\lambda_2$	-7.6	-7.7	-7.5	-7.5
$\lambda_3$	-21.0	-17.1	-15.0	-15.4
$\lambda_4$	-31.0	-26.1	-23.9	-25.6

**Fig. 9.9** Comparison of channel capacity and LTE physical layer throughput of  $2 \times 2$  setups for three different transmit antenna configurations

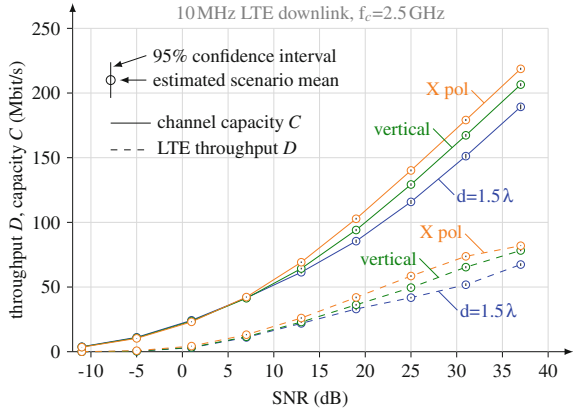
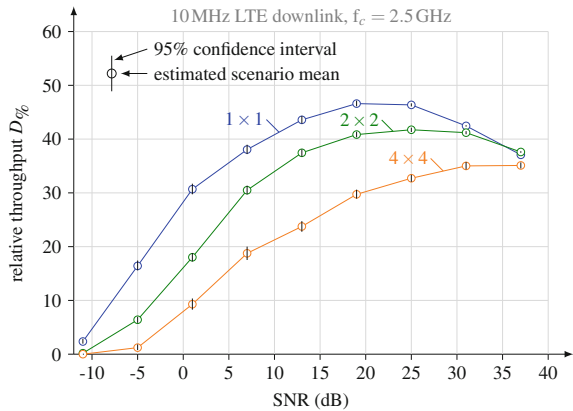


**Fig. 9.10** Comparison of  $1 \times 1$ ,  $2 \times 2$  (cross polarized) and  $4 \times 4$  ( $d = 10 \lambda$ ) in terms of relative throughput. The LTE throughput reaches nearly half of the channel capacity for  $1 \times 1$  transmissions and decreases with increasing number of transmit antennas



relative throughput as the ratio of throughput and capacity:  $D_{\%}(P_S) = 100 \cdot \frac{D(P_S)}{C(P_S)}$ . In Fig. 9.10 we show a comparison of the respectively best performing antenna configurations in terms of relative throughput. For all different numbers of transmit antennas the relative throughput increases with SNR and reaches a maximum as the maximum data rates defined in the LTE standard are reached. This maximum decreases with increasing number of transmit antennas as the overhead increases.

### 9.4 Measurements at High Velocities

LTE is designed to support user velocities of up to 500 km/h whereas mobile communications experiments in high mobility environments such as high speed trains, motorways or airplanes are expensive and time-consuming. Although such experiments are feasible, they are not well suited to, for example, directly compare different transmission techniques or to measure at different velocities or SNRs. Such

experiments require a fully controllable setup that allows for repeated transmissions under identical environmental conditions where all parameters are fixed except the one whose effect is being tested. In order to perform such experiments, the Vienna MIMO testbed was extended by antennas on the tip of a rotary unit [12, 13] that allows for fully controllable and repeatable measurements at velocities of up to 400 km/h. In this section, we give an overview of this measurement setup before the results of a measurement campaign comparing different channel interpolation methods for the LTE UL are presented.

### 9.4.1 Measurement Setup and Methodology

In our setup, as it is shown in Fig. 9.11, repeatable time-variant channels are generated by rotating the receive antennas around a central pivot. The received signals are then fed through the rod to rotary joints mounted inside the axis and are connected to the static receiver hardware of our testbed. A light barrier mounted on the axis captures the start of each turn of the rotating rod. This signal is connected to the trigger network of the testbed and triggers the signal transmission. Thereby, signal transmissions can be triggered at any desired angle of the rotating rod. The light barrier together with the trigger network allows for repeated transmissions over the same time-varying channel. Examples when multiple transmissions over the same channel are needed are:

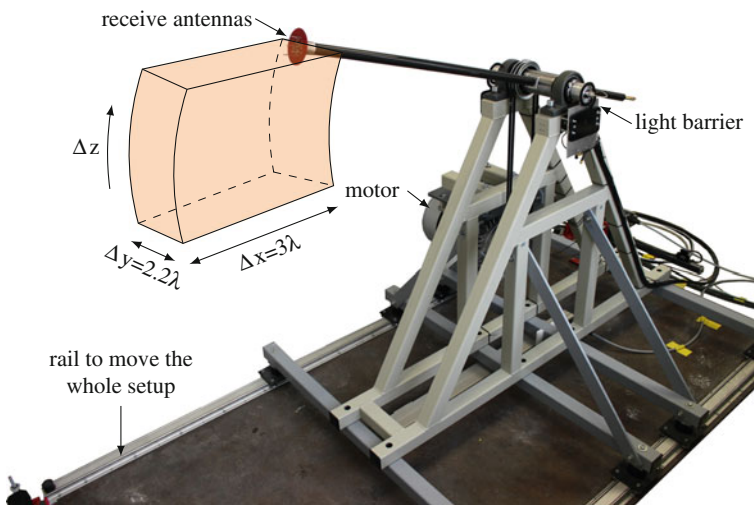


**Fig. 9.11** Measurement setup to generate repeatable time-variant channels

- Measurements at different SNRs. The same signals need to be transmitted with different transmit powers over the same channel.
- When comparing different transmit signals or transmit modes.
- Brute-force LTE measurements where different signals need to be transmitted over the same channel.
- Measurements with feedback, if feedback information should be applied to transmissions over the same channels to obtain the CSI. For measurements with feedback delay the trigger can be delayed according to the desired delay.
- Measurements at different velocities. As the spatial length  $\Delta z = T \cdot v$  of a signal with a certain temporal length  $T$  depends on the velocity  $v$ , it is not possible to transmit the same signal over the same channel at different velocities. Our approach for a fair comparison at different velocities is illustrated in Fig. 9.12. We transmit  $n$  realizations of the transmit signal of interest at the highest velocity. At half the maximum velocity, we transmit  $2n$  realizations and so forth.

In order to measure different channel realizations within the same scenario, the whole setup can be moved along the x and y-axis. The area where typical measurements are performed is illustrated by the box in Fig. 9.11. While  $\Delta x$  and  $\Delta y$  are given by mechanical constraints of the setup,  $\Delta z = T \cdot v$  depends on the length  $T$  of the transmit signals and the actual velocity  $v$ . Considering measurements at a velocity of  $v = 400$  km/h and the transmission of single LTE subframes having a length of  $T = 1$  ms, the length of the path the receive antennas move during the transmission calculates to  $\Delta z \approx 11$  cm. For the rod having a length of 1 m, the length of the path corresponds to an angle of about  $6^\circ$ . Figure 9.12 illustrates the path of the receive antennas and the corresponding bending of the path over 1 ms when moving at 400 km/h.

### 9.4.2 LTE Uplink Fast Fading Channel Interpolation

In the measurement campaign reported in [14] we were interested in the performance of different channel interpolation techniques for the LTE UL. Compared to the LTE

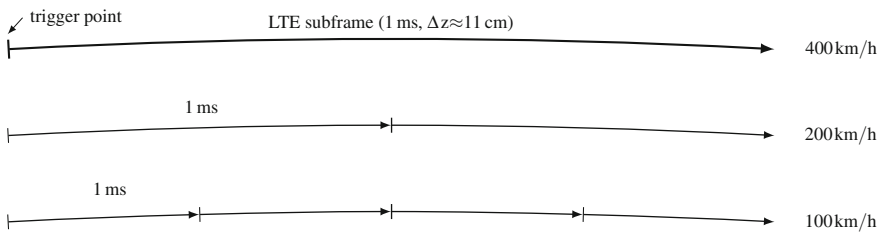


**Fig. 9.12** Trajectories of the receive antennas when transmitting LTE subframes. Multiple transmissions of the transmit signals at lower velocities allows for transmissions over the same spatial channels at different velocities

DL, the temporal spacing of the Demodulation Reference Signals (DMRS) in the UL is about twice the spacing as in the DL. Furthermore, if frequency-hopping is performed the number of adjacent pilots transmitted in a certain subband is two for inter-subframe frequency hopping and one for intra-subframe frequency hopping where frequency hopping is performed on a per-slot basis. Due to this special structure of pilot symbols, channel estimation in the LTE UL is a challenging problem. The authors of [15] proposed an interpolation algorithm based on adaptive order polynomial fitting to mitigate Inter-Carrier Interference (ICI), in [16] the polynomial basis expansion model is employed and the estimation accuracy is improved by an autoregressive model. Our idea is to include channel estimates from the previous and from the subsequent subframe into the process of channel interpolation. The additional delay that is introduced by applying channel estimates from the subsequent subframe is not considered.

**System Model**

We consider continuous single antenna LTE UL transmissions with frequency hopping being disabled. Sounding Reference Signals (SRS) and the Physical Uplink Control Channel (PUCCH) are both not considered. Figure 9.13 illustrates the resulting time/frequency resource grid for three consecutive resource blocks that consist only of data symbols and pilot symbols. At the receiver side we perform a symbol-by-symbol Least Squares (LS) channel estimation in the frequency domain and calculate the Zero Forcing (ZF) equalizer by the different interpolation methods under investigation. Although we do not perform frequency hopping, we emulate it by considering the cases where only one or two pilot symbols are used.

- *Average*: Averaging the channel estimates from pilot positions  $p_0$  and  $p_1$ . In the static case this method improves the channel estimation by 3 dB in terms of signal-to-noise ratio (SNR) but averages over temporal variations in the fast fading case.

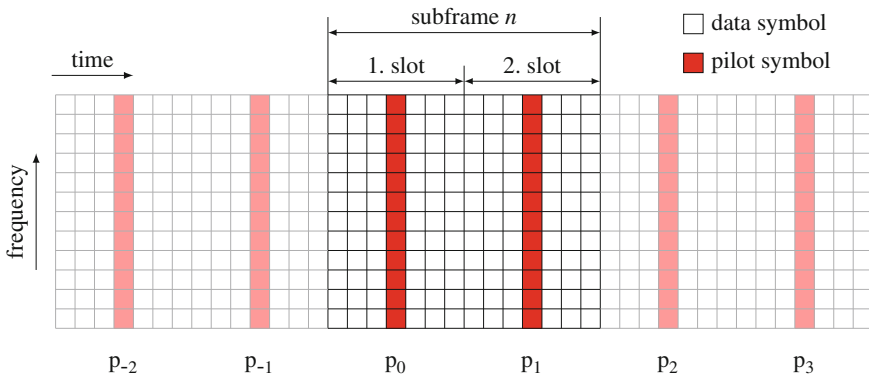


**Fig. 9.13** Resource grid of the LTE uplink. Due to SC-FDMA modulation, symbols marked as data symbols are the DFT-precoded data symbols rather than the actual data symbols

- *1 point*: Data symbols of slot  $n$  are equalized by the channel estimates from pilot at position  $p_n$ . This method is applicable in the case of intra-subframe frequency hopping.
- *2 point linear*: Linear interpolation and extrapolation based on the estimates at pilot position  $p_0$  and  $p_1$ . This method is applicable in the case inter-subframe frequency hopping is performed but intra-subframe frequency hopping is not activated.
- *4 point linear*: Linear interpolation based on the estimates at pilot position  $p_{-1}$ ,  $p_0$ ,  $p_1$  and  $p_2$ .
- *4 point spline*: Spline interpolation based on the estimates at pilot position  $p_{-1}$ ,  $p_0$ ,  $p_1$  and  $p_2$ .
- *6 point spline*: Spline interpolation using the estimates from pilot positions  $p_{-2}$  to  $p_3$ .

The resulting equalizers are then applied in the frequency domain on the DFT-precoded data symbols transmitted during subframe  $n$  in Fig. 9.13. The previous subframe and the subsequent subframe are only considered to obtain additional channel estimates.

**Measurement**

Both, the generation of transmit signals and the processing of the received signals is based on the Vienna LTE-A Uplink Link Level Simulator [17]. In order to measure the physical layer throughput by the brute-force approach described in Sect. 9.2, one subframe for each of the 15 different MCSs is pre-generated. Every subframe is repeated three times for transmissions at the maximum velocity of  $v = 400$  km/h whereas the central subframe  $n$  is the subframe to be decoded and the neighboring subframes  $n - 1$  and  $n + 1$  are used to obtain the additional channel estimates. At half of the maximum velocity (200 km/h) two subframes of interest ( $n$ ) are transmitted over the desired channel ( $\Delta z$ ) and so forth. Figure 9.14 illustrates this idea of transmitting over the same spatial channel at different velocities whereas the number of subframes considered in the evaluation is given by  $R(v) = \frac{400}{v}$  (Table 9.4).

**Table 9.4** Measurement parameters.

Center frequency	2.506 GHz ( $\lambda \approx 12$ cm)
Velocities	50, 100, 200 and 400 km/h
Channel realizations	49 (within an area of about $3 \lambda \times 2.2\lambda$ )
Transmission mode	10 MHz LTE UL, single antenna transmission, normal cyclic prefix, all resources scheduled for a single user, no SRS, no PUCCH
Modulation and coding	15 different MCSs according to the 15 different Channel Quality Indicators (CQIs) defined in the standard
Receiver	Single antenna, LS channel estimation, ZF equalization

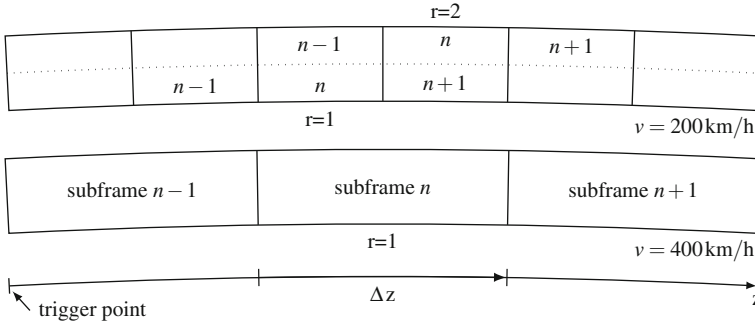


**Fig. 9.14** Transmitting over the same spatial channels allows for a fair comparison at different velocities

**Evaluation**

As figure of merit for the comparison of different channel interpolation methods the physical layer throughput is considered. Furthermore, the SNR as well as the Signal-to-Interference Ratio (SIR) and the Signal to Interference and Noise Ratio (SINR) as measures for the amount of ICI are evaluated.

**Physical Layer Throughput**

By using the brute-force approach perfect knowledge of the best performing MCS is emulated for every channel realization and every value of transmit power by transmitting all different MCSs over the same channel. The independent evaluation of all received signals then yields a value of throughput  $D_m$  for every combination of measurement parameters whereas  $k$  denotes the channel realization,  $r$  being the temporal repetition,  $v$  the velocity,  $P_S$  the transmit power and  $I$  the channel interpolation method. The throughput  $D_m$  is maximized over the different MCSs by

$$\widehat{D}_m(k, r, v, I, P_S) = \max_{\text{MCS}} D_m(k, r, v, I, P_S, \text{MCS}) \tag{9.4}$$

before the average throughput

$$D(v, I, P_S) = \frac{1}{K} \frac{1}{R(v)} \sum_{k=1}^K \sum_{r=1}^{R(v)} \widehat{D}_m(k, r, v, I, P_S) \tag{9.5}$$

is obtained by averaging over all  $K$  different channel realizations and  $R(v)$  temporal repetitions.

**SIR, SINR and SNR**

The power of each subcarrier is estimated in the frequency domain whereas we obtain the signal-plus-interference-plus-noise power  $P_{\text{SIN}}$  at data subcarrier positions, the interference-plus-noise power  $P_{\text{IN}}$  at the DC subcarrier where no data is transmitted



and the noise power  $P_V$  by measuring at the same subcarrier positions during a noise gap when no signal is transmitted. These thereby obtained power estimates are averaged similar to Eq. (9.5) separately over all channel realizations and temporal repetitions.  $P_{SIN}$  and  $P_{IN}$  are furthermore averaged over all different MCSs. The estimated SIR then calculates to

$$SIR(v, P_S) = \frac{\overline{P}_{SIN}(v, P_S) - \overline{P}_{IN}(v, P_S)}{\overline{P}_{IN}(v, P_S) - \overline{P}_V(v, P_S)}, \tag{9.6}$$

the SINR to

$$SINR(v, P_S) = \frac{\overline{P}_{SIN}(v, P_S) - \overline{P}_{IN}(v, P_S)}{\overline{P}_{IN}(v, P_S)}, \tag{9.7}$$

and the SNR to

$$SNR(v, P_S) = \frac{\overline{P}_{SIN}(v, P_S) - \overline{P}_{IN}(v, P_S)}{\overline{P}_V(v, P_S)}. \tag{9.8}$$

**Results**

The conditions in terms of SIR, SINR and SNR under which the measurement was performed are shown in Fig. 9.15. Due to the aforementioned methodology, the SNR is constant over the whole range of velocities. Comparing the SIR to analytical results [18], derived for two popular models, shows a higher SIR in our scenario. Both models, Jakes’ spectrum and the uniform model are based on uniformly distributed scattering objects which is not the case in our scenario. The SINR is upper bounded by noise at low velocities and upper bounded by the ICI power at high velocities. While we observe a large decrease of SINR for increasing velocity at high SNR, the SINR curve flattens for lower SNRs. The impact of ICI on the throughput becomes nearly independent of the velocity and the performance is rather determined by noise and the quality of the channel interpolation method than by ICI.

**Fig. 9.15** Channel conditions under which the measurement was performed

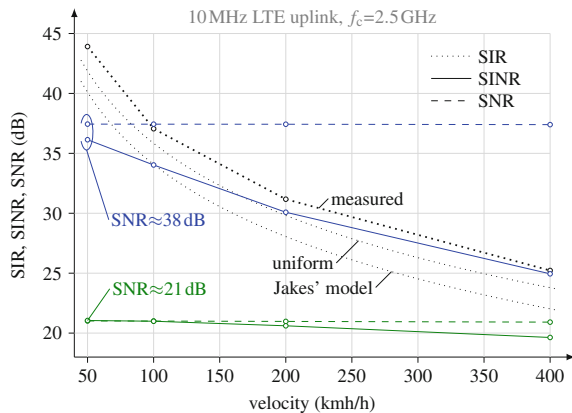


**Fig. 9.16** Measurement results comparing different channel interpolation methods in terms of throughput for two different values of transmit power resulting in an average SNR of **a**  $\approx 38$  dB and **b**  $\approx 21$  dB

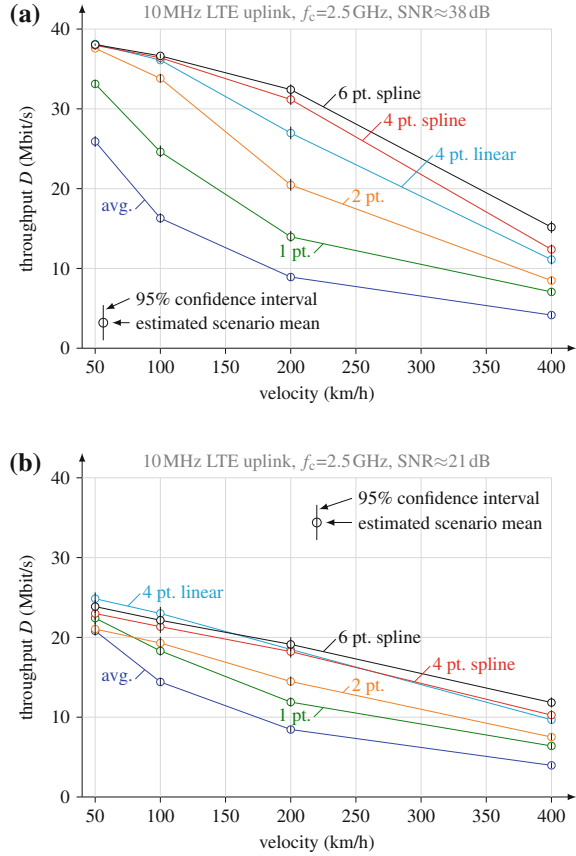


Figure 9.16 compares the considered channel interpolation methods in terms of physical layer throughput for two different values of SNR. As expected, the worst performance is observed when channel estimates from two pilots are averaged. The performance increases with the number of pilots in the channel interpolation. The highest gains at high SNR are observed between *1 point*, where no interpolation is performed and *2 point* interpolation and moreover when channel extrapolation in the *2 point* case is replaced by interpolation when performing *4 point linear* interpolation. Additional gains are observed when using spline interpolation, especially at high SNR and high velocities. At lower SNR, spline interpolation outperforms *4 point linear* interpolation only at moderate to high velocities. At low velocities, the gain of channel estimation SNR becomes visible for the *averaging* method as it performs as good as the *2 point* method. Furthermore, the throughput flattens at lower SNRs as the SINR flattens. At low velocities, the throughput is then determined by the SNR. The impact of the channel interpolation method is still visible at high velocities.

## References

1. M. Lerch, S. Caban, M. Mayer, M. Rupp, The Vienna MIMO testbed: evaluation of future mobile communication techniques. *Intel Technol. J.* **18**, 58–69 (2014)
2. S. Caban, A. Disslbacher-Fink, J.A. García Naya, M. Rupp, Synchronization of wireless radio testbed measurements, in *Proceedings of IEEE International Instrumentation and Measurement Technology Conference (I2MTC2011)* (2011). doi:[10.1109/IMTC.2011.5944089](https://doi.org/10.1109/IMTC.2011.5944089)
3. S. Caban, J.A. García Naya, M. Rupp, Measuring the physical layer performance of wireless communication systems. *IEEE Instrum. Meas. Mag.* **14**(5), 8–17 (2011). doi:[10.1109/MIM.2011.6041377](https://doi.org/10.1109/MIM.2011.6041377)
4. M. Mayer, G. Artner, G. Hannak, M. Lerch, M. Guillaud, Measurement based evaluation of interference alignment on the Vienna MIMO testbed, in *Proceedings of the Tenth International Symposium on Wireless Communication Systems (ISWCS'13)*, Ilmenau, 2013
5. S. Caban, J.A. García Naya, L. Castedo, C. Mehlführer, Measuring the influence of TX antenna spacing and transmit power on the closed-loop throughput of IEEE 802.16-2004 WiMAX, in *Proceedings of IEEE Instrumentation and Measurement Technology Conference (I2MTC2010)*, 2010
6. S. Caban, J.A. García Naya, C. Mehlführer, M. Rupp, Measuring the closed-loop throughput of 2x2 HSDPA over TX power and TX antenna spacing, in *Proceedings of 2nd International Conference on Mobile Lightweight Wireless Systems (Mobilight-2010)*, 2010
7. K. Werner, J. Furuskog, M. Riback, B. Hagerman, Antenna configurations for 4x4 MIMO in LTE—field measurements, in *71st IEEE Vehicular Technology Conference (VTC 2010-Spring)*, pp. 1–5, 2010. doi:[10.1109/VETECS.2010.5493762](https://doi.org/10.1109/VETECS.2010.5493762)
8. W. Xie, T. Yang, X. Zhu, F. Yang, Q. Bi, Measurement-based evaluation of vertical separation MIMO antennas for base station. *IEEE Antennas Wirel. Propag. Lett.* **11**, 415–418 (2012). doi:[10.1109/LAWP.2012.2194688](https://doi.org/10.1109/LAWP.2012.2194688)
9. M. Lerch, M. Rupp, Measurement-based evaluation of the lte mimo downlink at different antenna configurations, in *Proceedings of the 17th International ITG Workshop on Smart Antennas, WSA 2013*, Stuttgart, 2013
10. S. Schwarz, J.C. Ikuno, M. Simko, M. Taranetz, Q. Wang, M. Rupp, Pushing the limits of LTE: a survey on research enhancing the standard. *IEEE Access* **1**, 51–62 (2013). doi:[10.1109/ACCESS.2013.2260371](https://doi.org/10.1109/ACCESS.2013.2260371)
11. G. Foschini, M. Gans, On limits of wireless communications in a fading environment when using multiple antennas. *Wirel. Pers. Commun.* **6**, 311–335 (1998). doi:[10.1023/A:1008889222784](https://doi.org/10.1023/A:1008889222784)
12. S. Caban, J. Rodas, J.A. García-Naya, A methodology for repeatable, off-line, closed-loop wireless communication system measurements at very high velocities of up to 560 km/h, in *Proceedings of International Instrumentation and Measurement Technology Conference (I2MTC 2011)*, Binjiang, 2011. doi:[10.1109/IMTC.2011.5944019](https://doi.org/10.1109/IMTC.2011.5944019)
13. S. Caban, R. Nissel, M. Lerch, M. Rupp, Controlled OFDM measurements at extreme velocities, in *Proceedings of ExtremeCom'2014, Galapagos Islands, Ecuador*, 2014
14. M. Lerch, Experimental comparison of fast-fading channel interpolation methods for the LTE uplink, in *Proceedings of the 57th International Symposium ELMAR-2015, Zadar*, 2015. doi:[10.1109/ELMAR.2015.7334482](https://doi.org/10.1109/ELMAR.2015.7334482)
15. B. Karakaya, H. Arslan, H. Cirpan, Channel estimation for LTE Uplink in High Doppler Spread, in *Wireless Communications and Networking Conference (WCNC 2008)*, pp. 1126–1130, 2008. doi:[10.1109/WCNC.2008.203](https://doi.org/10.1109/WCNC.2008.203)
16. L. Yang, G. Ren, B. Yang, Z. Qiu, Fast time-varying channel estimation technique for LTE uplink in HST environment. *IEEE Trans. Vehic. Technol.* **61**(9), 4009–4019 (2012). doi:[10.1109/TVT.2012.2214409](https://doi.org/10.1109/TVT.2012.2214409)
17. J. Blumenstein, J.C. Ikuno, J. Prokopec, M. Rupp, Simulating the long term evolution uplink physical layer, in *Proceedings of the 53rd International Symposium ELMAR-2011, Zadar*, 2011
18. P. Robertson, S. Kaiser, The effects of Doppler spreads in OFDM (A) mobile radio systems. *IEEE Vehic. Technol. Conf. Fall* **1**, 329–333 (1999)